Strengthened Linkage between November/December North Atlantic Oscillation and Subsequent January European Precipitation after the Late 1980s

YANG LIU

Nansen-Zhu International Research Center, Institute of Atmospheric Physics, Chinese Academy of Sciences, and Climate Change Research Center, Chinese Academy of Sciences, Beijing, China

SHENGPING HE

Geophysical Institute, University of Bergen and Bjerknes Centre for Climate Research, Bergen, Norway

(Manuscript received 5 September 2019, in final form 6 July 2020)

ABSTRACT

This work investigates the nonsynchronous relationship between the North Atlantic Oscillation (NAO) and winter European precipitation. The results indicate that the linkage between early-winter (November and December) NAO and the following January precipitation and atmospheric circulation over the North Atlantic and European sectors became statistically significant after the late 1980s. Before the late 1980s, January precipitation and atmospheric circulation are weakly correlated with early-winter NAO. After the late 1980s, by contrast, the positive phase of the early-winter NAO is generally followed by an anomalous meridional dipole pattern with barotropic structure over the North Atlantic, which provides conditions for more (less) precipitation south of Iceland (east of the Azores). Further analysis elucidates that this regime shift may be partly attributed to the change of early-winter NAO, which is concurrent with significant change in the intensity of the synoptic and low-frequency eddy interaction over the Atlantic–European sectors. Anomalous positive sea level pressure and geopotential height, along with zonal wind anomalies associated with a positive early-winter NAO over the North Atlantic, are more significant and extend more northeastward after the late 1980s, which may be induced by an intensified transient eddy feedback after the late 1980s, as well as the enhanced storm-track activity over the North Atlantic. Thus, early-winter NAO can induce significant ocean temperature anomalies in the North Atlantic after the late 1980s, which extend downward into the middle parts of the thermocline and persist until the following January to trigger NAO-like atmospheric circulation patterns. Analyses from the Community Earth System Model large ensemble simulations indicate the effects of internal climate variability on such a strengthened linkage.

1. Introduction

The North Atlantic Oscillation (NAO), one of the most marked atmospheric modes of variability over the North Atlantic, features changes in atmospheric mass between the Arctic and the subtropical Atlantic (Wallace and Gutzler 1981; Barnston and Livezey 1987; Hurrell et al. 2003). Variations in the NAO have an important influence on society and environment (Czaja et al. 2003; Visbeck et al. 2003; Pinto and Raible 2012; Zhou et al. 2013; Zhou 2013). For example, the winter 2009/10 saw snowy and cold climate over most regions of the Northern Hemisphere, coinciding with the negative phase of the NAO (Orsolini et al. 2016). Even though the NAO is evident throughout the year, the climate anomalies associated with NAO are most dominant during boreal winter (Barnston and Livezey 1987; Hurrell et al. 2003). Changes in the NAO produce pronounced climate variations in the surrounding continental areas of North America, Europe, and North Africa and also in remote regions of the Arctic (van Loon and Rogers 1978; Barnston and Livezey 1987; Wibig 1999; Wu and Huang 1999; Gong et al. 2001; Wanner et al. 2001; Wu and Wang 2002; Gong and Ho 2003; Li et al. 2003; Yang et al. 2004; Jeong and Ho 2005; Oglesby et al. 2012). For instance, a positive winter NAO index is concurrent with a pronounced northward shift in the Atlantic storm activity (Rivière and Orlanski

Supplemental information related to this paper is available at the Journals Online website: https://doi.org/10.1175/JCLI-D-19-0662.s1.

Corresponding author: Shengping He, shengping.he@uib.no

DOI: 10.1175/JCLI-D-19-0662.1

2007), which causes intensified storm activity from southern Greenland across Iceland into northern Europe and weakened storm activity to the south (Hurrell et al. 2003). Consequently, there are often drier-than-normal and wetter-than-normal conditions over southern and northern Europe, respectively (Hurrell 1995; Hurrell and van Loon 1997). As for remote impacts of the NAO, Wu and Huang (1999) revealed that positive NAO leads to a weakened Siberian high and weakened East Asian winter monsoon, accompanied by significant positive temperature anomalies over the north of the Asian continent. Additionally, Xu et al. (2016) suggested that there is a linkage between the NAO and Eurasian climate in boreal winter, but such a linkage is unstable. Forecast skill has developed a lot and offers the possibility to assess North Atlantic climate and the NAO at seasonal lead times, which could bring great benefits to society by allowing plans to be made months in advance (Scaife et al. 2014; Svensson et al. 2015; Clark et al. 2017; Parker et al. 2019).

Changes in the NAO can also impact the allocation of evaporation and precipitation (Hurrell 1995; Dickson et al. 2000) on different time scales (Pinto and Raible 2012; Woollings et al. 2015). Several studies have adopted the NAO as a predictor of the precipitation over western Iberia in winter (Zorita et al. 1992; Corte-Real et al. 1995, 1998; Rodriguez-Puebla et al. 1998; González-Rouco et al. 2000; Trigo and Palutikof 2001). Trigo et al. (2004) revealed a negative relationship between the winter NAO index and the interannual variability of early-spring rainfall over the Iberian Peninsula, as well as the southern Italian region (Ferrari et al. 2013). It is noteworthy that the effect of the NAO on surface climate might be nonstationary. Rodó et al. (1997) uncovered an unstable relationship between the NAO and precipitation in Spain during winter. The NAO, which experienced a pronounced decadal change around the late 1970s, has a stronger connection with the boreal surface air temperature over East Asia (Sun et al. 2008; Yuan and Sun 2009) and the East Asian summer rainfall after the decadal change (Sun and Wang 2012). Some hypotheses have been proposed to explain the unstable relationship between the NAO and climate variability, including changes in the North Atlantic air–sea process in the thermohaline circulation (Walter and Graf 2002), solar activity (Gimeno et al. 2003), and intensity and position change in the NAO (Jung et al. 2003; Haylock et al. 2007; Vicente-Serrano and López-Moreno 2008).

Recently, several studies have indicated the delayed effect of the winter NAO on the subsequent seasonal climate. Qian and Saunders (2003) noted a significant relationship between the summer temperature over the British Isles and the preceding late-winter NAO index. The sea ice, sea surface temperature (SST), and snow-cover anomalies provide the memory for the persistent impact of winter NAO (Ogi et al. 2003, 2004; Zuo et al. 2016). Sung et al. (2006) revealed a possible delayed influence of the winter NAO on the East Asian summer monsoon precipitation. Recently, Bhatla et al. (2016) suggested that the spring NAO index is inversely correlated with the Indian summer monsoon rainfall.

Despite the above-mentioned work, few studies have investigated the delayed influence of the winter NAO on subseasonal time scale. Motivated by previous studies, we found that there is a strengthened connection between the early-winter (November and December) NAO index and the North Atlantic–European precipitation in the subsequent January after the late 1980s. Further efforts are also made to understand the possible mechanisms underlying this intensified connection.

2. Data and methods

a. Data

The monthly and daily means atmospheric variables used in our study are derived from the reanalysis data of the National Centers for Environmental Prediction–National Center for Atmospheric Research (NCEP–NCAR), with a horizontal resolution of 2.5° × 2.5° and 17 vertical pressure levels extending from 1000 to 10 hPa (Kalnay et al. 1996). The monthly precipitation data are obtained from NOAA's precipitation reconstruction (Chen et al. 2002). This precipitation dataset is gridded at a 2.5° latitude × 2.5° longitude resolution for the period from 1948 to present. Monthly mean SST data are from the Hadley Centre Sea Ice and Sea Surface Temperature (HadISST) dataset, which has a 1° × 1° resolution and spans the period from 1870 to the present (Rayner et al. 2003). The subsurface ocean temperature is obtained from Met Office Hadley Centre observations datasets (Good et al. 2013). We also made use of long-term observed precipitation such as the precipitation data provided by Climatic Research Unit (CRU; Harris et al. 2014) and the Global Precipitation Climatology Centre (GPCC; Becker et al. 2011), so as to support the results derived from reanalysis dataset. To investigate the effect of internal climate variability and external climate drivers, we also use the data from the large ensemble simulation by the Community Earth System Model (CESM-LE; Kay et al. 2015).

The observed NAO indices were obtained, respectively, from 1) the NOAA Climate Prediction Center (CPC) web site (http://www.cpc.ncep.noaa.gov/products/precip/CWlink/pna/nao.shtml; referred to herein as CPC_NAO), 2) the CRU (https://crudata.uea.ac.uk/cru/data/nao/; Jones et al. 1997; referred to as CRU_NAO), and

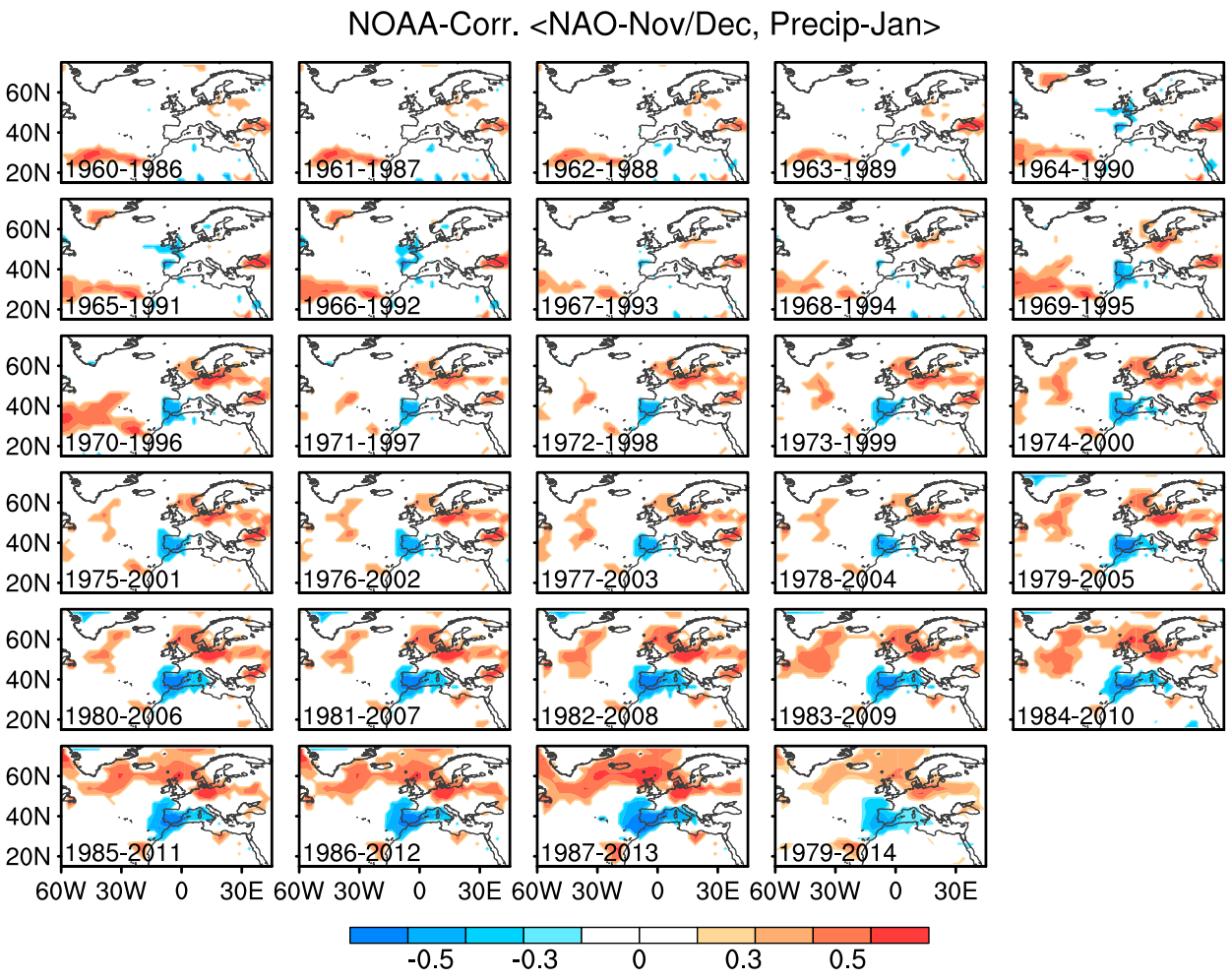

FIG. 1. The 27-yr sliding correlation between previous November/December NAO index and Atlantic–European precipitation of the following January during 1960–2014. Only significant values (at the 90% confidence level) are shown.

3) the Climate Analysis Section (https://climatedataguide.ucar.edu/climate-data/hurrell-north-atlantic-oscillation-nao-index-pc-based; Hurrell 1995; referred to as Hurrell_NAO). The NAO index from the CESM-LE simulations is defined as the difference of normalized SLP zonally averaged over 80°W–30°E at 35° and 65°N latitudes (Li and Wang 2003).

b. Methods

To qualitatively compute the influence of synoptic transient eddies on the zonal mean flow, the extended Eliassen–Palm (EP) flux (also called local EP flux) is applied in this study (Hoskins et al. 1983; Trenberth 1986; Lau 1988). Local divergence anomalies of extended EP flux are associated with cyclonic forcing to its north and anticyclonic forcing to its south (Lau 1988; Chen et al. 2018). Based on Trenberth (1986), the divergence of the extended EP flux corresponds to the feedback of transient eddies on the time mean flow, and the horizontal components of the extended EP flux can be represented as $\mathbf{E} = [(1/2)(\overline{v'^2} - \overline{u'^2})\mathbf{i}, -\overline{u'v'}\mathbf{j}] \times \cos\varphi$. Here overbars denote time averages, and the primes represent synoptic-scale parts of the flow; u and v represent the zonal and meridional wind components, respectively. A bandpass filter with a time scale of 2–8 days is applied to obtain the synoptic-scale part of the flow (Chen et al. 2018).

3. Change in the early-winter NAO–January precipitation connection

To evaluate the connection between the winter NAO and precipitation in Europe, we calculate the 27-yr sliding correlation of the winter (November–January) NAO index with January and February precipitation anomalies. We find that the relationship between the

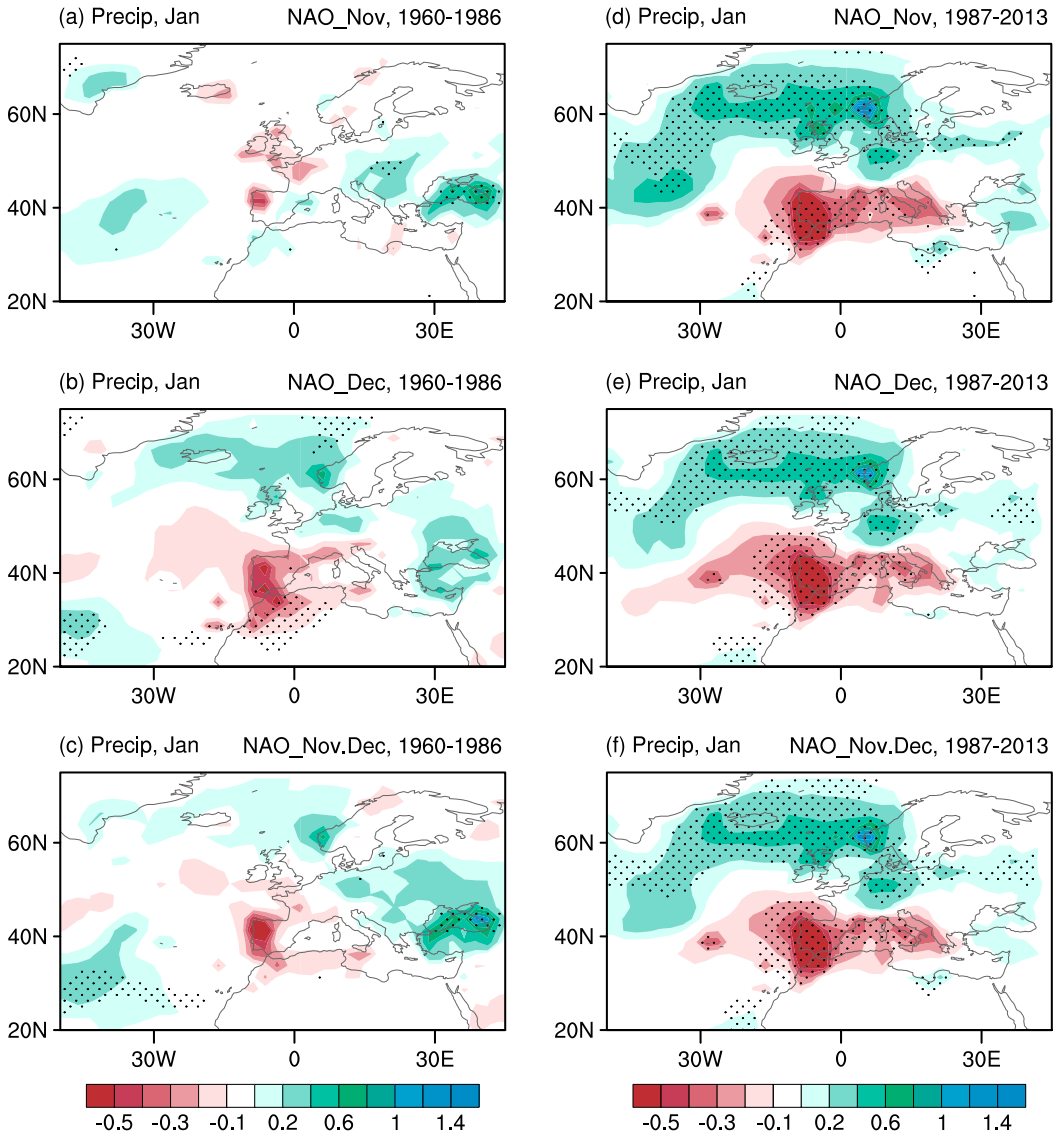

FIG. 2. Regression maps of January precipitation onto the (a) November, (b) December, and (c) November/December NAO index during 1960/61–1986/87. (d)–(f) As in (a)–(c), respectively, but during 1987/88–2013/14. Stippled regions denote the values significant at the 95% confidence level based on a two-tailed Student's *t* test.

January NAO and January North Atlantic–European precipitation is stable, which is consistent with previous studies (Hurrell 1995; Hurrell and van Loon 1997). Interestingly, it is found that there is an increasing in the relationship between the early-winter NAO index and the North Atlantic–European precipitation in the following January and it becomes more statistically significant after the later 1980s (Fig. 1). Therefore, we select two subperiods, 1960/61–1986/87 (P1) and 1987/88–2013/14 (P2), to illustrate the interdecadal change in the relationship of early-winter NAO and European precipitation.

Figure 2 shows the regressed maps of the January precipitation over the North Atlantic–Europe sector onto the November, December, and November–December mean (November/December) NAO index during the two subperiods. During P1, there are only a few positive anomalies in January distributed over the eastern Black Sea following positive November NAO (Fig. 2a). During P2 (Fig. 2d) the January precipitation anomalies related to November NAO show a meridional dipole pattern, with significant positive values over north of the Iceland expanding northeast toward Europe and significant negative values over the southern part of the North Atlantic–Europe sector. As for the December and November/December NAO, the regressed January precipitation anomalies also display an apparent dipole

pattern over the North Atlantic–Europe sector during P2 (Figs. 2e,f). By contrast, the January precipitation anomalies related to the December and November/December NAO during P1 are tenuous (Figs. 2b,c), indicating a strengthened linkage of January precipitation with the preceding early-winter NAO after the late 1980s. Given the close resemblance between the results associated with November and December NAO, the following analyses focus mainly on the results associated with the early-winter mean NAO (i.e., November/December NAO). Additionally, the differences of regressed map between the two periods are significant, which is verified by Monte Carlo test and a field significance test (Figs. S1 and S2 in the online supplemental material).

A precipitation index (PI) is defined as the difference of area-averaged precipitation between the regions of 50°–75°N, 40°W–10°E and 30°–45°N, 20°W–15°E. First, we examined the 27-yr sliding correlation coefficients between early-winter NAO and January PI during 1960–2014 (blue curve in Fig. 3). It indicates a continuous strengthening of early-winter NAO–January PI relationship, with a transition to a statistically significant relationship after the late 1980s. We further extended the analyses via the long-term datasets. It is indicated that the relationship between the early-winter NAO and the January precipitation increases since the 1940s and becomes statistically significant since the late 1980s. Such a conclusion does not change with different datasets (Fig. 3) and with different gliding windows (such as 11, 21, and 31 years) (Fig. S3).

We further present the regressed maps of January atmospheric circulation conditions onto the November/December NAO during the two subperiods. During P1, related to anomalous November/December NAO, almost no statistically significant atmospheric circulation anomalies appear over the Atlantic–Europe sectors in the following January (Figs. 4a–c). By contrast, corresponding to an increase of one standard deviation of November/December NAO index during P2, the January sea level pressure (SLP) anomaly shows a significant decrease of 3–4 hPa in the Icelandic region and an increase of 3–4 hPa over the Azores (Fig. 4d, contours), indicating an enhancement of the subtropical Azores high and polar Icelandic low. Correspondingly, a pair of surface anticyclonic and cyclonic anomalies appear over the Azores and Iceland, respectively, accompanied by significant westerlies prevailing from the North Atlantic to west of Europe along high latitudes (around 60°N) (Fig. 4d, vectors), which contributes more (less) warm moist air from north of Atlantic to northern (southern) parts of Europe. At 500 hPa, consistent with lower-level circulation anomalies, there is also a dipole pattern in geopotential height anomaly over the North

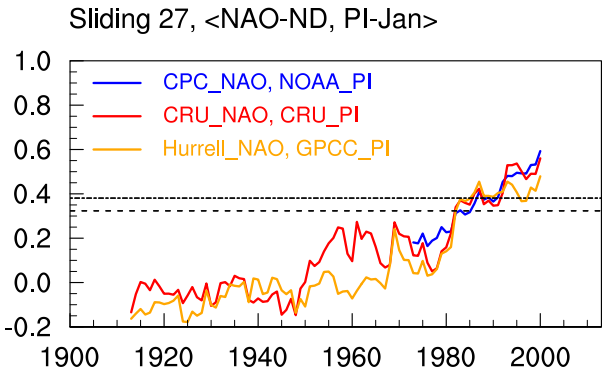

FIG. 3. The 27-yr sliding correlation between early-winter NAO and January PI. Blue line indicates the correlation between the CPC_NAO and the PI calculated from NOAA precipitation during 1960–2014; red line indicates the correlation between the CRU_NAO and the PI calculated from the precipitation data from CRU during 1900–2014; and orange line indicates the correlation between the Hurrell_NAO and the PI calculated from the precipitation data from GPCC during 1900–2014. The long- (short-) dashed lines indicate the results are significant at the 90% (95%) confidence level.

Atlantic (Fig. 4e). This circulation dipole pattern in Figs. 4d and 4e exhibits a near-equivalent barotropic structure from the surface to the middle troposphere. Associated with the enhancing of the subtropical Azores high and the polar Icelandic low, anomalous westerlies and easterlies prevail aloft at 300 hPa around 55° and 35°N, respectively (Fig. 4f). It is noteworthy that the pattern correlation of the November/December NAO-related SLP anomalies in January over 10°–80°N, 60°W–60°E with those in November–December mean is 0.44 in P1 and 0.74 in P2 (Fig. S4), implying more persistence of November/December NAO after the late 1980s. Further evidences are listed in Table 1, which shows that 1) the correlation coefficients of NAO indexes between November and December is 0.71 during P2, and 2) the correlation coefficients of January NAO index with the preceding November NAO, December NAO, and November–December mean NAO indexes are 0.48, 0.58, and 0.58 in P2, whereas the correlation coefficients in P1 are not statistically significant.

After the late 1980s, the January precipitation anomalies could be induced by the significant anomalous anticyclonic circulation over the North Atlantic (Fig. 4d). As indicated by the vertically integrated water vapor transport anomalies, there is more (less) moisture transported from the North Atlantic to north (south) Europe due to the strong anomalous westerly (easterly) jet over north (south) of the anomalous anticyclone over the North Atlantic (Fig. 5b). By contrast, the November/December NAO-related water vapor anomalies are statistically insignificant over the North Atlantic–Europe sector during P1 (Fig. 5a).

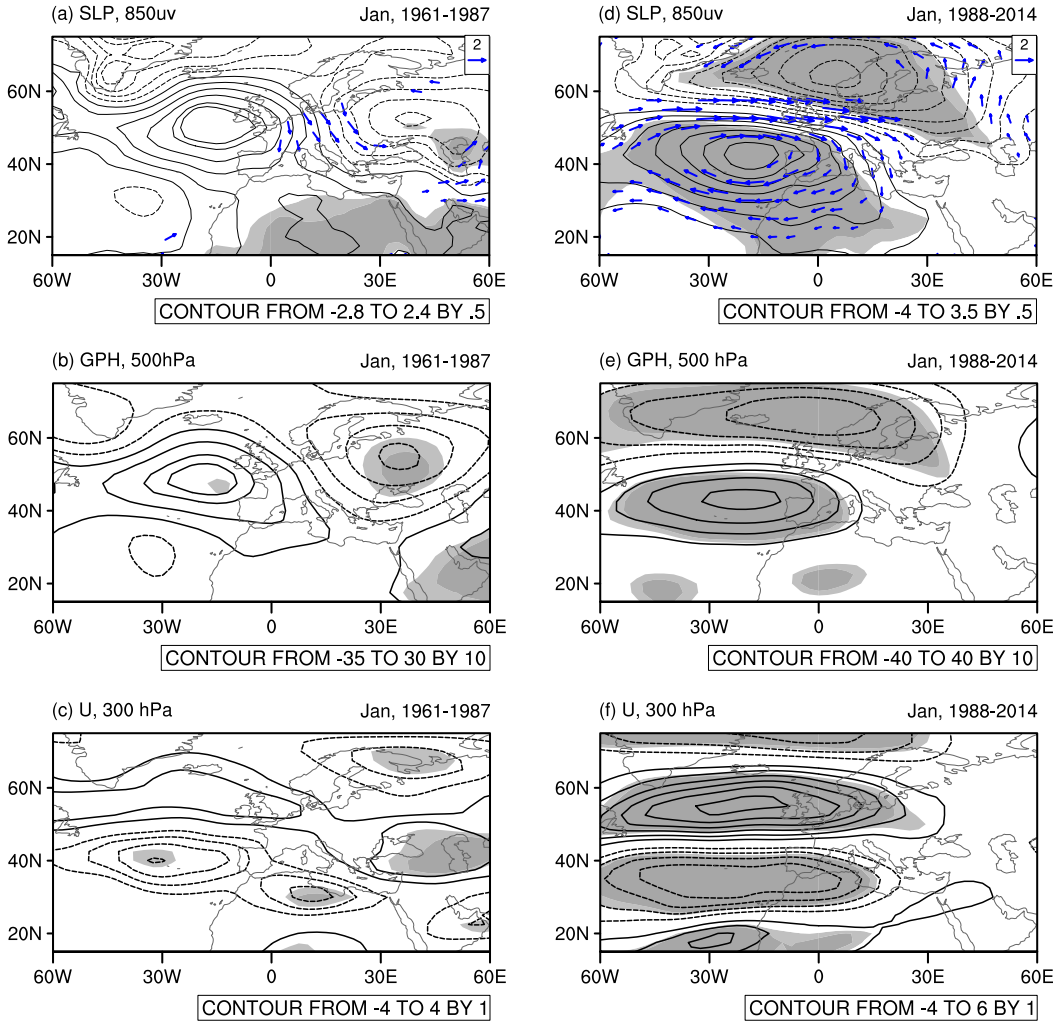

FIG. 4. Regression maps of following January (a) 850-hPa wind (vectors) and SLP (contours), (b) 500-hPa geopotential height, and (c) 300-hPa zonal wind onto the November/December NAO index during 1960/61–1986/87. (d)–(f) As in (a)–(c), respectively, but during 1987/88–2013/14. Light and dark shaded values are significant at the 90% and 95% confidence levels based on a two-tailed Student's *t* test. Vectors in (a) and (d) are significant at the 95% confidence level based on a two-tailed Student's *t* test.

Consistent with anomalous water vapor transport conditions, anomalous vertical motions occur over the North Atlantic–Europe sector. As shown in Fig. 6a, the January vertical motion shows a weak connection with the November/December NAO during P1. However, during P2 (Fig. 6b), a north–south dipole structure of vertical motion anomalies is evident at midlatitudes of the North Atlantic. The significant anomalous upward (downward) motions extend throughout the entire troposphere aloft around 60°N (40°N), which agrees with the situation of stronger than normal Icelandic low (Azores high). Such anomalous upward (downward)

TABLE 1. Correlation coefficients of early-winter (November, December, and 2-month mean) NAO indexes (referred to as NAO-N, NAO-D, and NAO-ND, respectively) with the following January NAO index (referred to as NAO-J). Asterisks (*) indicate the correlation coefficients are statistically significant at the 95% confidence level based on a two-tailed Student's *t* test.

	NAO-N, NAO-D	NAO-N, NAO-J	NAO-D, NAO-J	NAO-ND, NAO-J
P1	0.01	−0.16	0.28	0.09
P2	0.71*	0.48*	0.58*	0.58*

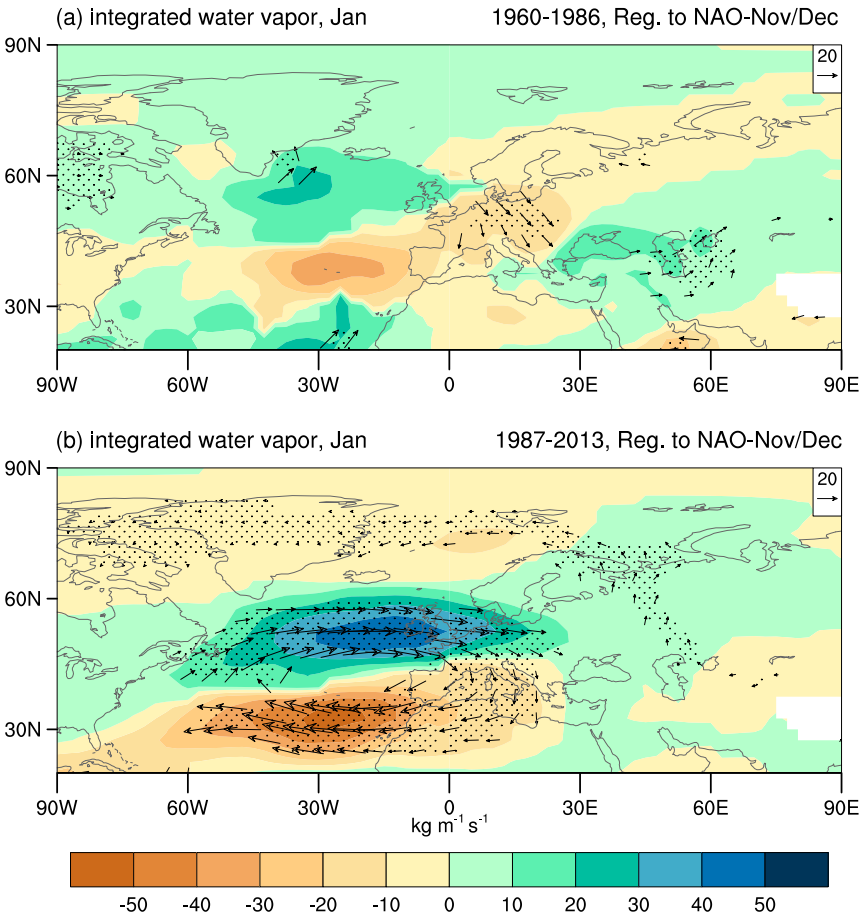

FIG. 5. Regression maps of vertically (from the surface to 300 hPa) integrated water vapor transport vector ($kg\,m^{-1}\,s^{-1}$) anomalies for the period of (a) 1960/61–1986/87 and (b) 1987/88–2013/14 January onto the November/December NAO. The color shading indicates the magnitude of the vertically integrated water vapor transport vector. Vectors and stippled regions indicate the vectors and magnitude anomalies are significant at the 95% confidence level based on a two-tailed Student's *t* test.

motions centered at 60°N (40°N) are consistent with the precipitation increments (decrements) over northwestern Europe (Iberian Peninsula). Given that the change of precipitation is related to the cloudiness, we present, in Figs. 6c and 6d, the maps of anomalous total cloud cover in January with respect to preceding November/December NAO. Corresponding to the positive phase of November/December NAO, the distribution of anomalous total cloud cover is not significant during P1 (Fig. 6c). However, after the late 1980s, an extratropical "north–south" anomaly dipole pattern is distinct in total cloud cover over Europe (Fig. 6d). Such change of the cloud cover is highly consistent with the variation in water vapor and vertical motion anomalies. The significant change in January atmosphere related to the November/December NAO supports the strengthened relationship of January precipitation over the North Atlantic–Europe sector with the preceding early-winter NAO after the late 1980s.

4. Possible mechanisms

Why is there such a strengthened connection of early-winter NAO and January precipitation over the North Atlantic–Europe sector? To answer this question, we first examine the spatial structure of the November/December NAO in different periods. Figure 7 illustrates the NAO-related SLP and geopotential height anomalies in November/December during the two subperiods. As expected, the pattern of simultaneous SLP anomalies bears a resemblance to the positive phase of the NAO during both periods; however, the positive anomalous center over the North Atlantic extends more eastward during P2 than that during P1 (cf. Figs. 7b and 7a, and 7d

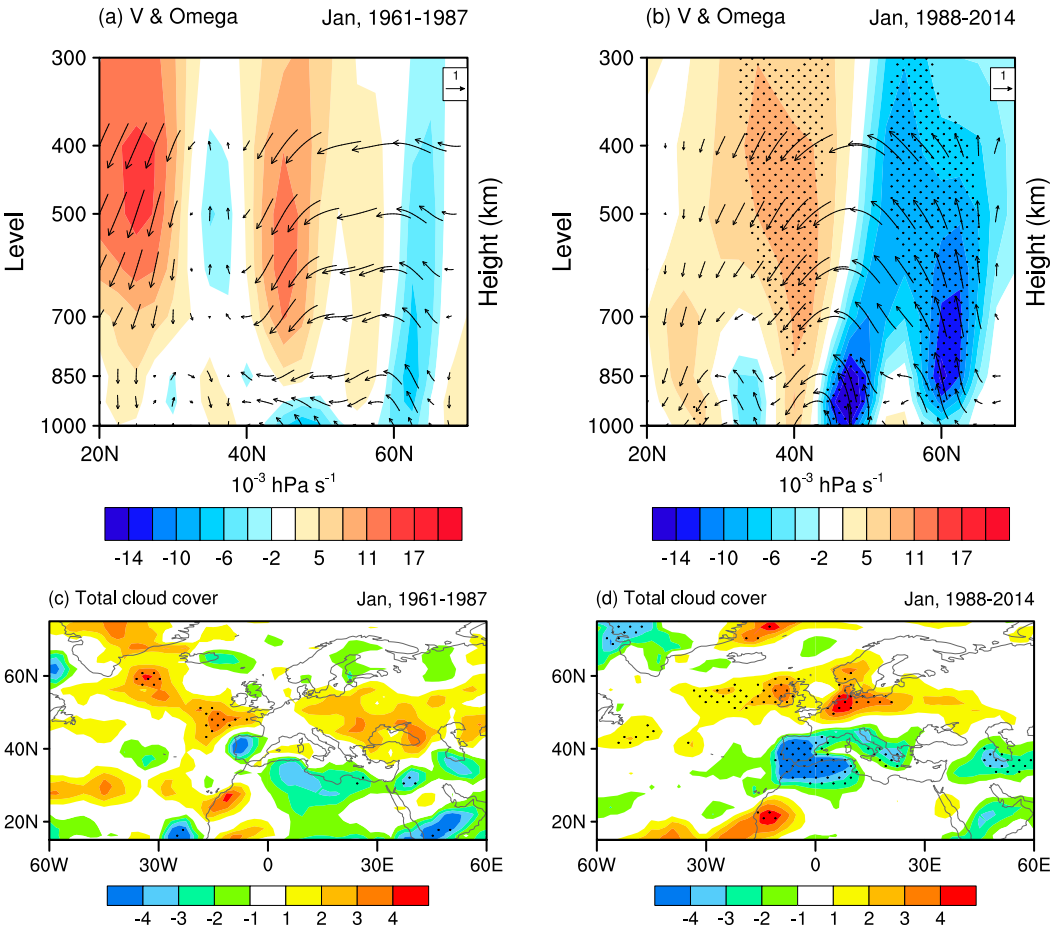

FIG. 6. Latitude cross section (averaged over 10°W–0°) for regression maps of January zonally averaged wind (vectors) and vertical velocity (shaded; in Pa s^{-1}) anomalies during (a) 1960/61–1986/87 and (b) 1987/88–2013/14 onto the November/December NAO index. Also shown are regression maps of following January total cloud cover during (c) 1960/61–1986/87 and (d) 1987/88–2013/14 onto the November/December NAO index. Stippled regions indicate the anomalies are significant at the 95% confidence levels based on a two-tailed Student's *t* test.

and 7c). This might promote significant low-level wind anomalies stretching from the North Atlantic eastward toward Europe (Fig. 8b). In contrast, positive anomalies of both SLP and geopotential height related to the NAO retreat westward and are confined to the North Atlantic region during P1 (Figs. 7a,c,e). Correspondingly, significant low-level wind anomalies over the North Atlantic–Europe sectors also retreat westward to west of 30°E (Fig. 8a). It also suggests that the atmospheric circulation anomalies related to the NAO over the Northern Hemisphere show a higher degree of zonal symmetry during P2 than that during P1, which is further supported by the increasing of the zonal symmetry index (ZSI) of the NAO (Liu and Wang 2013) (Fig. S5). Moreover, early-winter NAO has larger amplitude during P2 (with a variance of 0.97) than during P1 (with a variance of 0.49). This implies that the different structures and amplitude of November/December NAO are possibly responsible for the interdecadal change in the relationship between the early-winter NAO and following January precipitation over the North Atlantic–Europe sector.

Previous studies suggested that the interaction of high and low frequency is a decisive internal source of anomalous mean flow (Lau 1988; Limpasuvan and Hartmann 2000; Lorenz and Hartmann 2003; Chen et al. 2018). By diagnosing the terms in the streamfunction-tendency equation, Feldstein (2003) showed that NAO life cycle is dynamically driven by transient eddy fluxes, associated with storm-track activity (Blackmon 1976). Meanwhile, the poleward shift of midlatitude storm-track activity during winter is also linked to the poleward shift of precipitation in midlatitude regions, and is also tied to the intensity of the NAO (Yin 2005). Therefore, we investigate if there are differences in the eddy feedback between the two subperiods. Figure 9 presents early-winter NAO-related

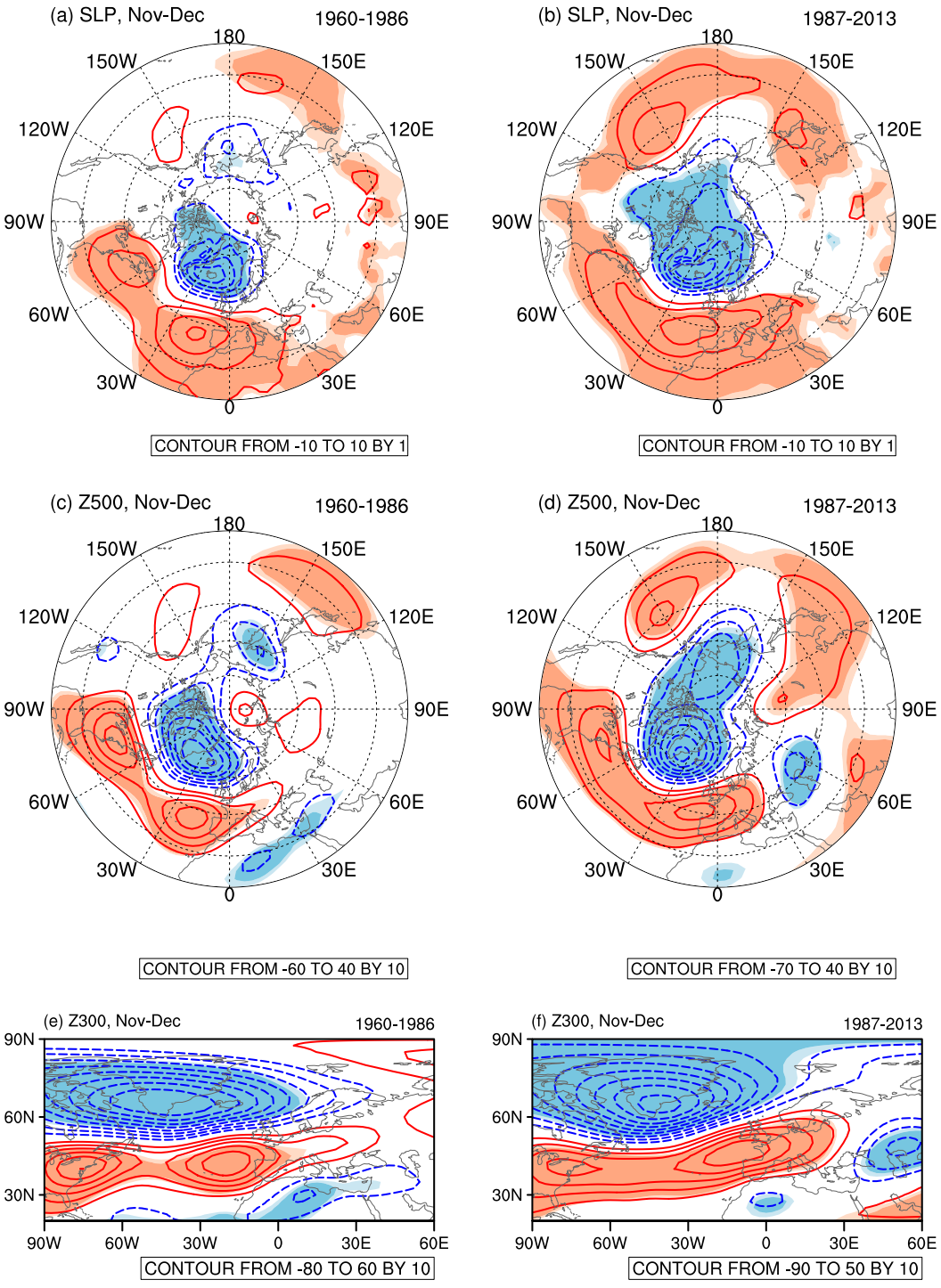

FIG. 7. Regression maps of November/December SLP anomalies onto the November/December NAO index during (a) 1960–86 and (b) 1987–2013. (c),(d) and (e),(f) As in (a),(b), but for geopotential height anomalies at 500 and 300 hPa, respectively. Light and dark shaded values are significant at the 90% and 95% confidence levels based on a two-tailed Student's *t* test.

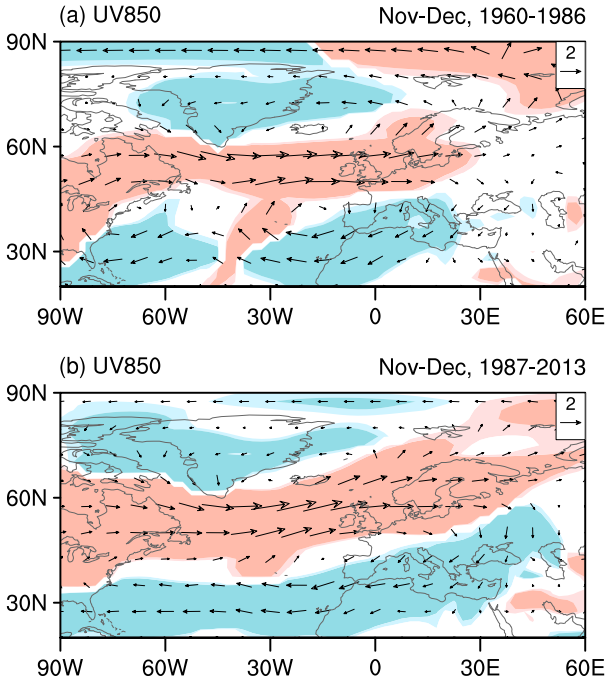

FIG. 8. Regression maps of November/December wind anomalies at 850 hPa onto the November/December NAO index during (a) 1960–86 and (b) 1987–2013. Light and dark shaded values are significant at the 90% and 95% confidence levels based on a two-tailed Student's *t* test.

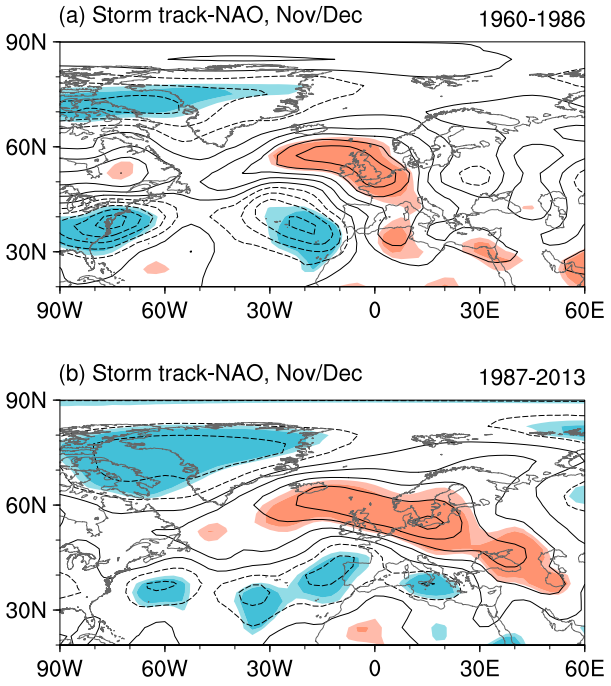

FIG. 9. Regression maps of November/December storm-track activity anomalies at 300 hPa onto the November/December NAO index during (a) 1960–86 and (b) 1987–2013. Light and dark shaded values are significant at the 90% and 95% confidence levels based on a two-tailed Student's *t* test. Contour intervals are 2 m in (a) and (b).

300-hPa storm-track activity anomalies over the North Atlantic for the two epochs. In this study, storm-track activity is represented by the root-mean-square of bandpass-filtered (2–8 days) geopotential height at 300 hPa (Lee et al. 2012; Chen et al. 2018). During P2, notable storm-track activity anomalies are observed zonally over the Iceland extending eastward to the Caspian Sea, which is characterized by significant positive anomalies over high latitudes (approximately 60°N) and negative anomalies over midlatitudes (approximately 30°N) (Fig. 9b). This accords with the anomalous configuration of the zonal wind over the North Atlantic–Europe sector, along with easterly and westerly anomalies over middle and high latitudes, respectively (Fig. 7f). As shown by existing literature (Lau 1988; Chen et al. 2018), positive storm-track activity anomalies are tied to cyclonic eddy forcing to its north and anticyclonic eddy forcing to its south. This might be related to the eastward stretching anomalies of atmospheric circulation over the North Atlantic–Europe sector (Figs. 7b,d,f and 8b). During P1, by contrast, the configuration of anomalous storm-track activity is weak over European region (Fig. 9a). Meanwhile, both the positive and negative anomalies of storm-track activity shift westward and are confined to the North Atlantic (Fig. 9a), in agreement with the westward retreated wind and geopotential height anomalies (Figs. 7a,c,e and 8a).

The distinct pattern of November/December storm-track activity associated with the NAO between the two subperiods may be attributed to the interdecadal change of the storm-track intensity over the North Atlantic (Jin et al. 2006a,b; Jin 2010). We demonstrate the time-mean November/December storm-track activity over the North Atlantic before and after the late 1980s. Although the two spatial patterns of climatological mean storm-track activity in the two subperiods are similar over the North Atlantic (Figs. 10a,b), the intensity of storm-track activity is stronger during P2 than that during P1. This feature is more notable by inspecting the storm-track activity difference between two periods (Fig. 10c), which indicates that the North Atlantic storm-track activity is significantly stronger during P2.

To further demonstrate the effects of transient eddies on the time-mean flow, we calculated the local EP flux. Figure 11 shows the NAO-related November/December extended EP flux and its divergence anomalies regressed during the two subperiods. The region of the storm track over the North Atlantic around 50°N shows significant anomalous divergent EP flux, which, however, is more dominant during P2 (cf. Figs. 11b and 11a), indicating

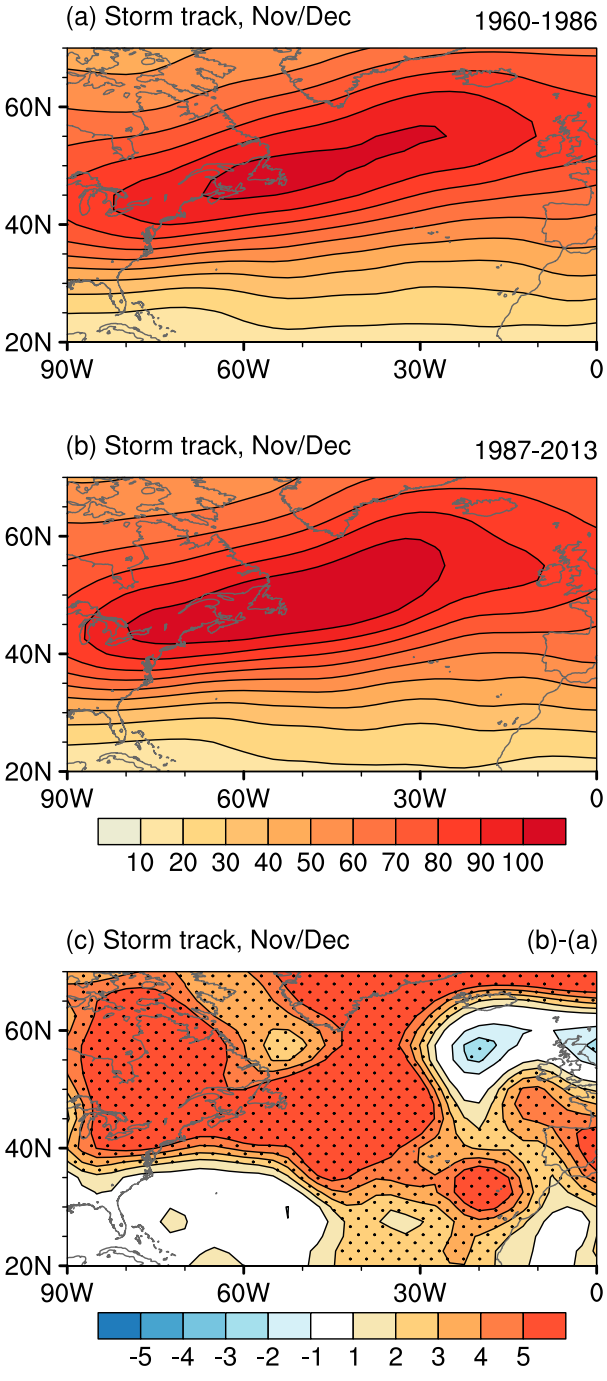

FIG. 10. Climatological distribution of storm-track activity at 300 hPa during (a) 1960–86 and (b) 1987–2013. (c) Difference in climatological storm-track activity between 1987–2013 and 1960–86. Stippled regions indicate the anomalies are significant at the 95% confidence levels based on a two-tailed Student's *t* test.

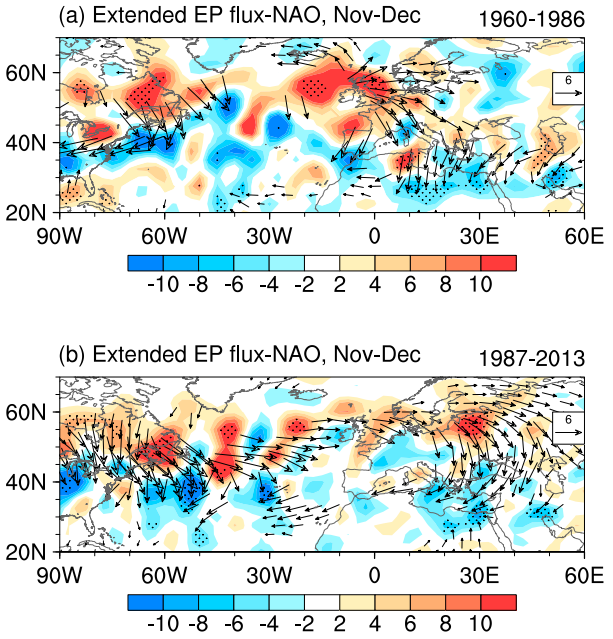

FIG. 11. Regression maps of November/December extended EP flux (vectors) and their divergence (shading) anomalies at 300 hPa onto the November/December NAO index during (a) 1960–86 and (b) 1987–2013. The presence of vectors and stippled regions indicate the anomalies are significant at the 95% confidence levels based on a two-tailed Student's *t* test.

that the eddies are more effective to accelerate the zonal wind. Besides, significant divergent and convergent anomalies are observed over eastern Europe and the Mediterranean during P2, respectively (Fig. 11b), while anomalous divergence is confined to the North Atlantic during P1 (Fig. 11a). The dominant differences of extended EP flux between the two subperiods are located in the regions where different NAO-related circulation emerges (Figs. 7 and 8).

Studies showed that the NAO has a significant intrinsic persistence (Czaja and Frankignoul 2002), but only has a short-term memory (less than one month) due to the chaotic nature of the atmospheric motion (Wang et al. 2000; Ogi et al. 2003). So how can the early-winter NAO have a delayed connection with the following January precipitation over the Euro-Atlantic sectors? Storm tracks are located over the midlatitude North Atlantic, where SST gradients are the largest in the Gulf Stream regions (Matsumura et al. 2019). The extratropical atmosphere has an important impact on the underlying SST, but it can produce a feedback to the atmosphere, especially in winter season (Kushnir et al. 2002). Hence, the air–sea feedback may be a possible candidate for the persistence of atmospheric anomalies. Figures 12 and 13 illustrate the evolution of the SST and turbulent heat flux anomalies associated with the early-winter NAO during the two subperiods. Corresponding to positive NAO index in November, anomalous upward (downward) turbulent heat fluxes coincide with cooling (warming) SST anomalies (SSTAs) in both

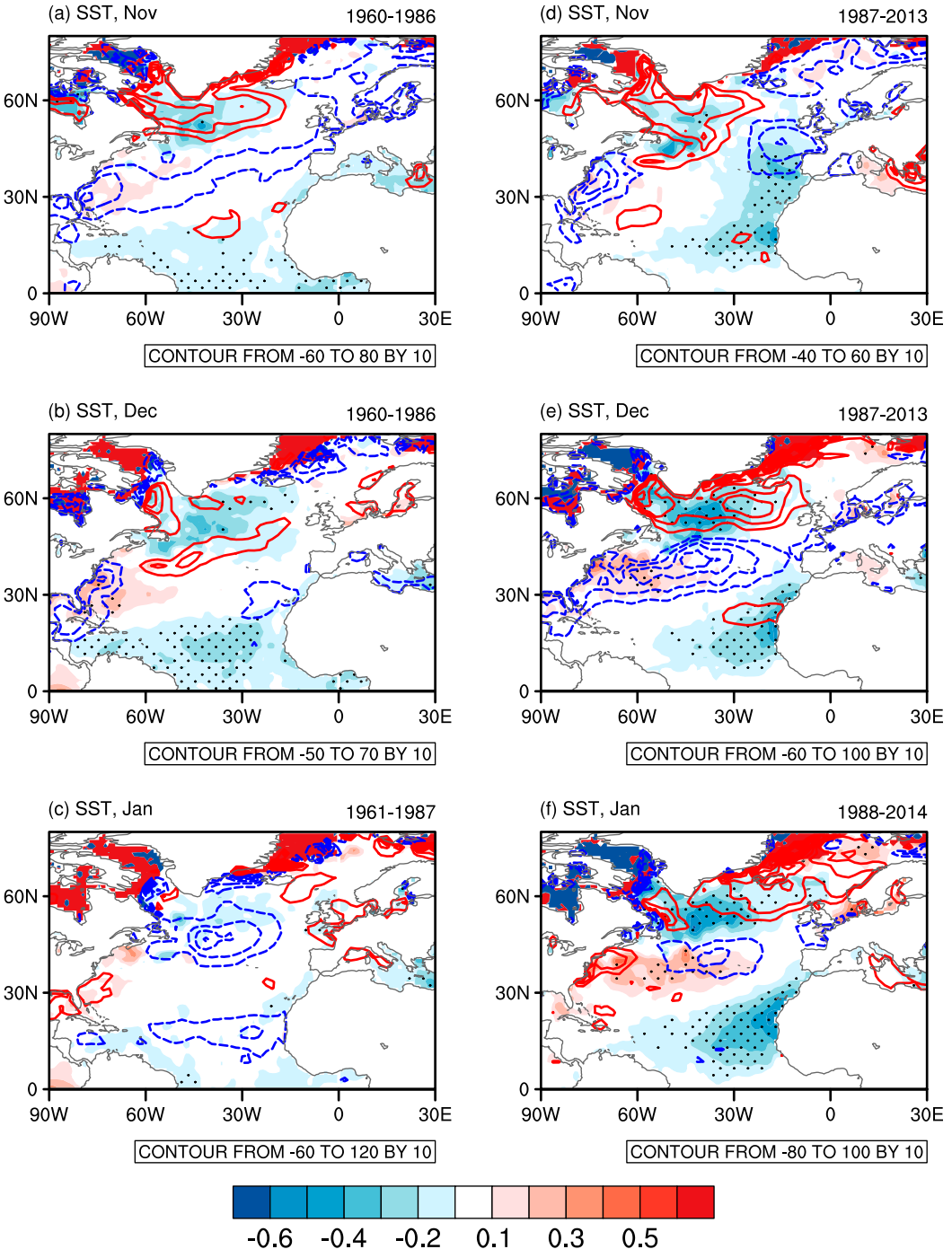

FIG. 12. Regression maps of (a) November, (b) December, and (c) the following January SST (shading; °C) and turbulent heat flux (contours; latent plus sensible, W m^{-2}; positive values indicate upward heat fluxes) anomalies onto the November NAO index during 1960/61–1986/87. (d)–(f) As in (a)–(c), respectively, but during 1987/88–2013/14. Stippled regions indicate the anomalies are significant at the 95% confidence levels based on a two-tailed Student's *t* test.

November and December (NAO leads by 1 month) in the midlatitude North Atlantic, indicating that the extratropical atmosphere forces the variations in SST in this region (Figs. 12a,b,d,e), which agrees well with previous studies (Seager et al. 2000; Kushnir et al. 2002; Pan 2005; Gulev et al. 2013). During P2, the tripole pattern of SSTAs, which is not remarkable in November, becomes remarkable in the following December and

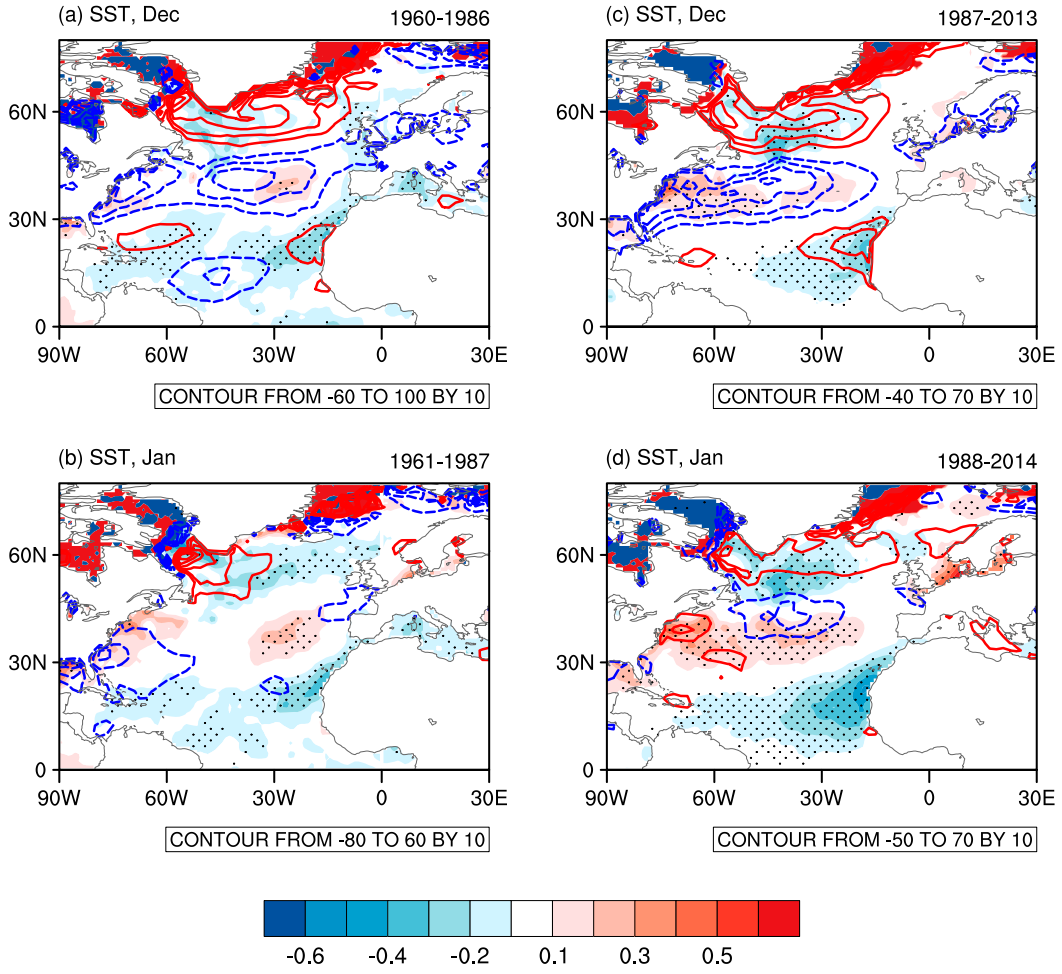

FIG. 13. Regression maps of (a) December and (b) the following January SST (shading; °C) and turbulent heat flux (contours; latent plus sensible; W m^{-2}; positive values indicate upward heat fluxes) anomalies onto December NAO index during 1960/61–1986/87. (c),(d) As in (a) and (b), respectively, but during 1987/88–2013/14. Stippled regions indicate the anomalies are significant at the 95% confidence levels based on a two-tailed Student's *t* test.

January (NAO leads by 1 and 2 months), suggesting that the NAO-related atmosphere develops the SSTAs tripole-like pattern (Figs. 12e,f). When it comes to January P2 (Fig. 12f), the tripole SSTA pattern develops and upward heat flux anomalies appear in the positive SSTA region (off the East Coast of the United States), reflecting the atmospheric response to the SSTA tripole pattern. Besides, positive heat flux anomalies off Newfoundland and in the subtropics become weaker than early winter. However, during P1, the SSTAs tripole pattern is not well developed over the extratropical North Atlantic in winter (Figs. 12a–c). In terms of the situation of December NAO, the tripole-like SSTAs appear in December and develop in January during P2 (Figs. 13c,d), but not P1 (Figs. 13a,b). From the view of dynamics, we assume that a positive feedback mechanism might play a vital role after the late 1980s between atmospheric circulation and the North Atlantic SST. The SSTAs tripole pattern is well established in January during P2 but not P1, indicating a stronger-than-normal linkage of early winter NAO and the following January SSTAs in the North Atlantic. Triggered by a simultaneous well-developed SSTAs tripole pattern, the positive NAO-like pattern in the following January further exerts its impact on the precipitation anomaly over North Atlantic as well as the European region. Similar results can be gained as well by using NOAA Extended Reconstructed SST version 4 data (Huang et al. 2015), so the results are reliable and not data dependent. It should be noted that such a tripole SSTA pattern in the North Atlantic can extend downward into the middle parts of the thermocline during P2 (Figs. 14 and 15), which further explains why the early-NAO signals can persist into the following January.

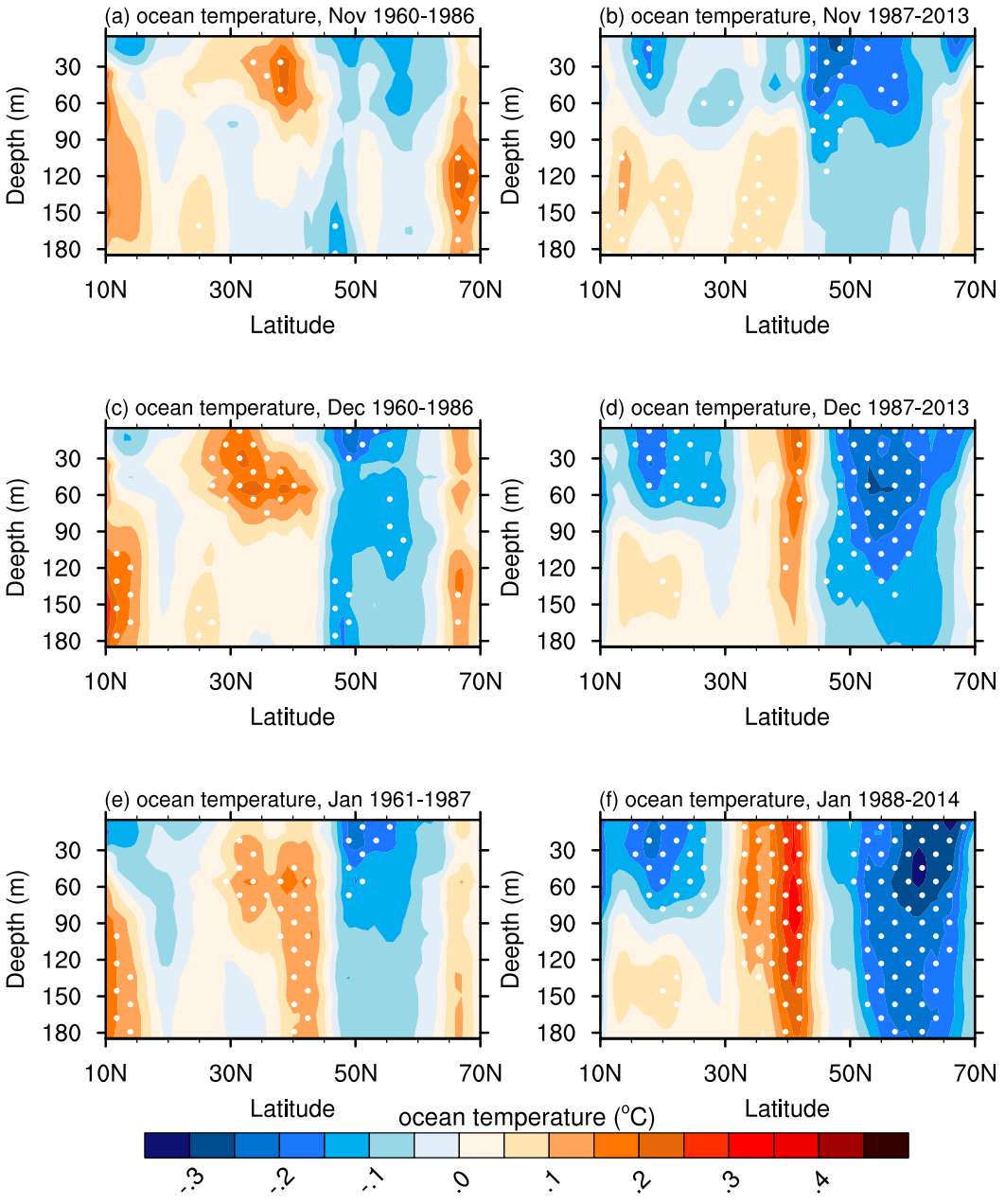

FIG. 14. Regression maps of (a) November, (b) December, and (c) the following January ocean temperature zonally averaged over 70°W–0° (shading; °C) onto the November NAO index during 1960/61–1986/87. (d)–(f) As in (a)–(c), respectively, but during 1987/88–2013/14. Stippled regions indicate the anomalies are significant at the 95% confidence levels based on a two-tailed Student's *t* test.

5. Conclusions and discussion

In the present study, we investigate the relationship of the early-winter NAO with the North Atlantic and European precipitation during the following January. There is a significant relationship between early-winter NAO and the following January precipitation anomalies after the late 1980s. Based on this result, we further compare the regression of the following January precipitation associated with the November, December, and 2-month averaged NAO index between before and after the late 1980s. It is suggested that after the late 1980s, a positive phase of early winter NAO favors wetter-than-normal January conditions south of Iceland and drier-than-normal conditions over the Iberian Peninsula and North Africa. Regression analysis revealed that following a stronger-than-normal early winter NAO event during P2,

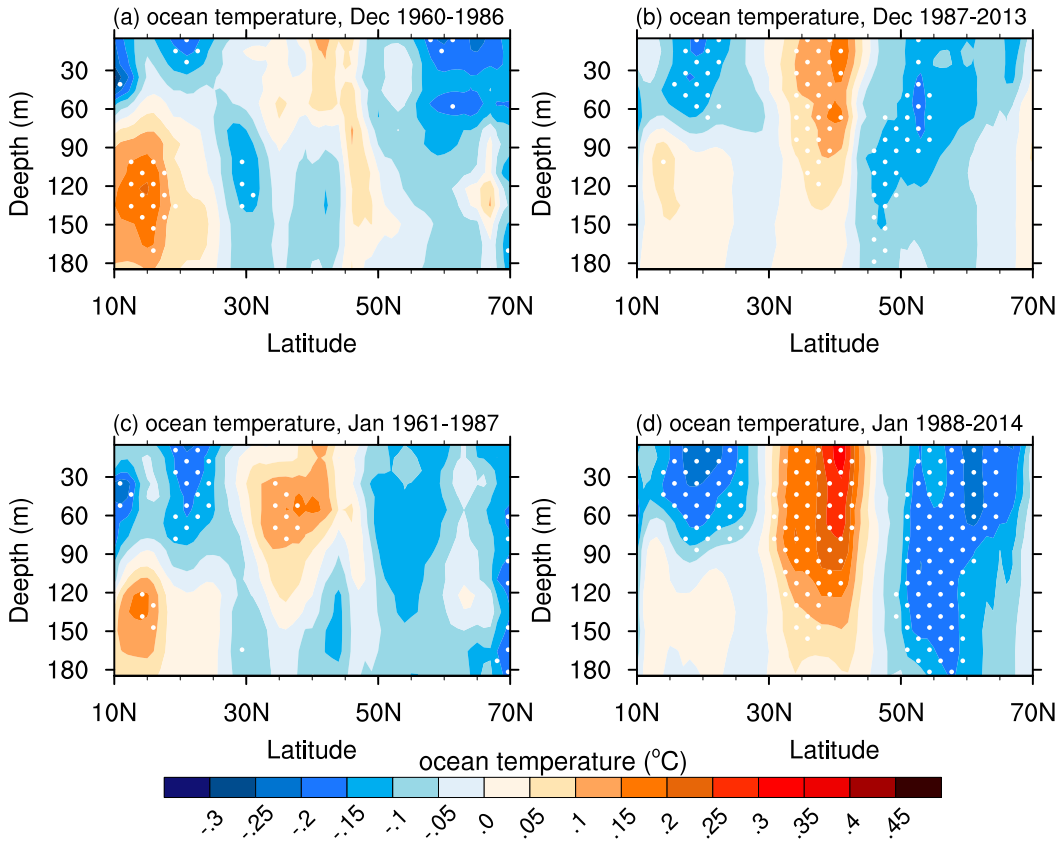

FIG. 15. As in Fig. 14, but for the ocean temperature zonally averaged over 70°W–0°.

the SLP field in the subsequent January shows a distinct intensification of the Icelandic low and Azores high, accompanied by westerly anomalies south of Iceland and northeasterly anomalies along the eastern flank of the Azores high. Meanwhile, significant positive (negative) 500-hPa geopotential height anomalies are located over the Azores (Iceland) and anomalous westerlies prevail over the northern part of Europe. These atmospheric anomalies in January have impacts on the variations of vertically integrated water vapor transport, vertical motion, and total cloud cover over the North Atlantic–Europe sector. By contrast, this situation is barely observed in January P1. Therefore, there is a significant connection between the preceding November and December NAO and the precipitation in Europe and coastal areas during the following January after the late 1980s.

Further work clarifies that the interdecadal change in the relationship between previous NAO and January precipitation over the North Atlantic and Europe may be partly ascribed to the regime shift of early winter NAO, which is related to the intensity of the synoptic and low-frequency eddy interaction. Figure 16 shows a schematic diagram of possible mechanisms for this nonsimultaneous relationship after the late 1980s. During P2, the configuration of anomalous SLP displays a high degree of zonal symmetry structure over Northern Hemisphere with a larger amplitude NAO. During P1, however, the pattern of SLP anomalies is detected

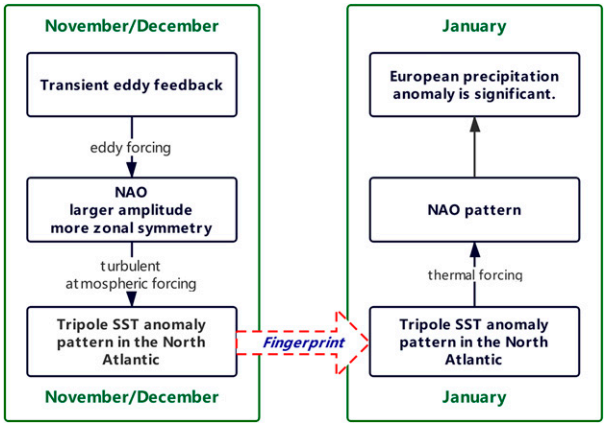

FIG. 16. Schematic diagram of possible physical mechanisms that contribute to the connection of the preceding November and December NAO with the following January precipitation anomaly pattern after the late 1980s.

locally over the North Atlantic with a smaller amplitude of NAO. Furthermore, the intensity of storm-track activity, from a feeble regime to a robust regime around the late 1980s, leading to the regime shift of NAO-related atmospheric circulation distribution. Meanwhile, SSTAs have been thought to be partly responsible for changes in atmospheric circulation over the North Atlantic–Europe sector in winter or spring (Namias 1964; Ratcliffe and Murray 1970; Davies et al. 1997). The "negative–positive–negative" SSTAs tripole pattern in the North Atlantic related to the simultaneous NAO could develop to the following January and generates a feedback onto the atmospheric circulation in the following January during P2. As a result, an NAO-like pattern emerges in January following an anomalous November/December NAO event and eventually has a lagged impact on the climate in North Atlantic and Europe.

The variability of the NAO's pattern, which has been explored by many studies (Hurrell 1995; Hilmer and Jung 2000; Jung et al. 2003; Peterson et al. 2003; Alonso-Perez et al. 2011; Woollings et al. 2015, 2018; Parker et al. 2019), might be responsible for the unstable influence on surface climate. However, there is no consensus on explaining the reason for the interdecadal change in NAO (Bader et al. 2011). Vicente-Serrano and López-Moreno (2008) suggest that the unstable relationship of the NAO across Europe is associated with the interdecadal shifts in the location of the positions of the NAO pressure centers. Climate model simulations show that the anthropogenic forcing can force a poleward shift of the jet stream and a dipole pattern of zonal wind anomalies with westerly anomalies over northern Europe and easterly anomalies over North Africa (Woollings and Blackburn 2012). It implies that the external forcing might influence the relationship between NAO and climate on subseasonal time scale. Figure 17 shows the 27-yr sliding correlation between the November/December NAO and January precipitation indexes during 1920–2080 in CESM-LE. First, individual ensemble members display both significant and insignificant correlations with fluctuation between positive and negative values. We further selected the ensemble members that have reproduced the time evolution of the observed correlation between November/December NAO and January precipitation indexes. The ensemble mean of correlations in the selected individual ensemble members shows a strengthened relationship of the November/December NAO with the January 1) precipitation (Fig. 17a: blue curve) and 2) surface heat flux, SST (Fig. S7), and SLP (Fig. S8) after the late 1980s. It implies the potential effect of internal climate variability on the relationship between

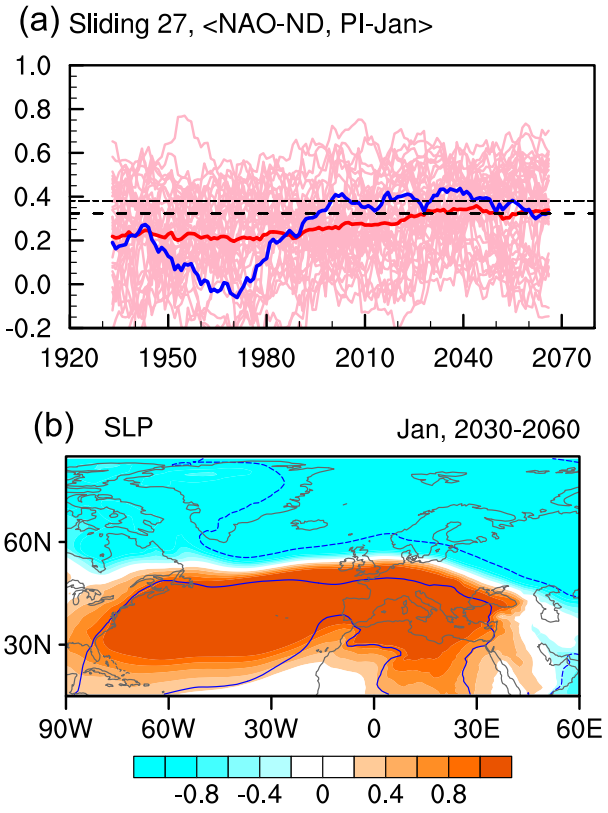

FIG. 17. (a) The 27-yr sliding correlation between previous November/December NAO and January P1 in CESM-LE: the thin red lines shows the results of 40 individual ensemble members; the thick red line shows the ensemble-mean correlations, and the thick blue line shows the results of individual members that match the observations. (b) Regression maps of following January SLP (shading) onto the normalized November/December NAO index during 2030–60 in the 40-ensemble mean. Values enclosed by blue contours are significant at the 90% confidence levels based on a two-tailed Student's *t* test.

November/December NAO and January precipitation indexes.

On the other hand, the ensemble mean of sliding correlations among 40 members shows strengthening as the external forcing increases, which becomes statistically significant after the mid-twenty-first century. The regression map of the following January SLP onto the normalized November/December NAO index during 2030–60 in the 40-member ensemble mean shows clearly a positive phase of NAO. But it is not the effect of a forced trend on both early winter NAO and January precipitation variability that contributes to their strengthened relationship in the observation, since such an intensified relationship remains after both the forced (ensemble mean) response in the early NAO and the forced (ensemble mean) response in January precipitation have been removed (Fig. S6b).

Acknowledgments. This research was supported by the National Key R&D Program of China (2016 YFA0600703), the National Natural Science Foundation of China (Grants 41875118, 41605059, 41421004), and the CONNECTED project supported by UTFORSK Partnership Program (UTF-2016-long-term/10030).

REFERENCES

Alonso-Perez, S., E. Cuevas, C. Perez, X. Querol, J. Baldasano, R. Draxler, and J. De Bustos, 2011: Trend changes of African airmass intrusions in the marine boundary layer over the subtropical eastern North Atlantic region in winter. *Tellus*, **63B**, 255–265, https://doi.org/10.1111/j.1600-0889.2010.00524.x.

Bader, J., M. D. Mesquita, K. I. Hodges, N. Keenlyside, S. Østerhus, and M. Miles, 2011: A review on Northern Hemisphere sea-ice, storminess and the North Atlantic Oscillation: Observations and projected changes. *Atmos. Res.*, **101**, 809–834, https://doi.org/10.1016/j.atmosres.2011.04.007.

Barnston, A. G., and R. E. Livezey, 1987: Classification, seasonality and persistence of low-frequency atmospheric circulation patterns. *Mon. Wea. Rev.*, **115**, 1083–1126, https://doi.org/10.1175/1520-0493(1987)115<1083:CSAPOL>2.0.CO;2.

Becker, A., P. Finger, A. Meyer-Christoffer, B. Rudolf, and M. Ziese, 2011: GPCC full data reanalysis version 6.0 at 1.0: Monthly land-surface precipitation from rain-gauges built on GTS-based and historic data. Global Precipitation Climatology Centre (GPCC), accessed January 2020, https://doi.org/10.5676/DWD_GPCC/FD_M_V7_100.

Bhatla, R., A. K. Singh, B. Mandal, S. Ghosh, S. N. Pandey, and A. Sarkar, 2016: A influence of North Atlantic Oscillation on Indian summer monsoon rainfall in relation to Quasi-Binneal [sic] Oscillation. *Pure Appl. Geophys.*, **173**, 2959–2970, https://doi.org/10.1007/s00024-016-1306-z.

Blackmon, M. L., 1976: A climatological spectral study of the 500 mb geopotential height of the Northern Hemisphere. *J. Atmos. Sci.*, **33**, 1607–1623, https://doi.org/10.1175/1520-0469(1976)033<1607:ACSSOT>2.0.CO;2.

Chen, M., P. Xie, J. E. Janowiak, and P. A. Arkin, 2002: Global land precipitation: A 50-yr monthly analysis based on gauge observations. *J. Hydrometeor.*, **3**, 249–266, https://doi.org/10.1175/1525-7541(2002)003<0249:GLPAYM>2.0.CO;2.

Chen, S., R. Wu, and W. Chen, 2018: A strengthened impact of November Arctic oscillation on subsequent tropical Pacific sea surface temperature variation since the late-1970s. *Climate Dyn.*, **51**, 511–529, https://doi.org/10.1007/s00382-017-3937-x.

Clark, R. T., P. E. Bett, H. E. Thornton, and A. A. Scaife, 2017: Skilful seasonal predictions for the European energy industry. *Environ. Res. Lett.*, **12**, 024002, https://doi.org/10.1088/1748-9326/aa57ab.

Corte-Real, J., X. Zhang, and X. Wang, 1995: Downscaling GCM information to regional scales: A non-parametric multivariate regression approach. *Climate Dyn.*, **11**, 413–424, https://doi.org/10.1007/BF00209515.

——, B. Qian, and H. Xu, 1998: Regional climate change in Portugal: Precipitation variability associated with large-scale atmospheric circulation. *Int. J. Climatol.*, **18**, 619–635, https://doi.org/10.1002/(SICI)1097-0088(199805)18:6<619::AID-JOC271>3.0.CO;2-T.

Czaja, A., and C. Frankignoul, 2002: Observed impact of Atlantic SST anomalies on the North Atlantic Oscillation. *J. Climate*, **15**, 606–623, https://doi.org/10.1175/1520-0442(2002)015<0606:OIOASA>2.0.CO;2.

——, A. W. Robertson, and T. Huck, 2003: The role of Atlantic Ocean–atmosphere coupling in affecting North Atlantic Oscillation variability. *The North Atlantic Oscillation: Climatic Significance and Environmental Impact*, *Geophys. Monogr.*, Vol. 134, Amer. Geophys. Union, 147–172.

Davies, J. R., D. P. Rowell, and C. K. Folland, 1997: North Atlantic and European seasonal predictability using an ensemble of multidecadal atmospheric GCM simulations. *Int. J. Climatol.*, **17**, 1263–1284, https://doi.org/10.1002/(SICI)1097-0088(199710)17:12<1263::AID-JOC191>3.0.CO;2-1.

Dickson, R. R., and Coauthors, 2000: The Arctic Ocean response to the North Atlantic Oscillation. *J. Climate*, **13**, 2671–2696, https://doi.org/10.1175/1520-0442(2000)013<2671:TAORTT>2.0.CO;2.

Feldstein, S. B., 2003: The dynamics of NAO teleconnection pattern growth and decay. *Quart. J. Roy. Meteor. Soc.*, **129**, 901–924, https://doi.org/10.1256/qj.02.76.

Ferrari, E., T. Caloiero, and R. Coscarelli, 2013: Influence of the North Atlantic Oscillation on winter rainfall in Calabria (southern Italy). *Theor. Appl. Climatol.*, **114**, 479–494, https://doi.org/10.1007/s00704-013-0856-6.

Gimeno, L., L. de la Torre, R. Nieto, R. Garcìa, E. Hernández, and P. Ribera, 2003: Changes in the relationship NAO–Northern Hemisphere temperature due to solar activity. *Earth Planet. Sci. Lett.*, **206**, 15–20, https://doi.org/10.1016/S0012-821X(02)01090-7.

Gong, D. Y., and C. H. Ho, 2003: Arctic Oscillation signals in the East Asian summer monsoon. *J. Geophys. Res.*, **108**, 4066, https://doi.org/10.1029/2002JD002193.

——, S. W. Wang, and J. H. Zhu, 2001: East Asian winter monsoon and Arctic Oscillation. *Geophys. Res. Lett.*, **28**, 2073–2076, https://doi.org/10.1029/2000GL012311.

González-Rouco, J. F., H. Heyen, E. Zorita, and F. Valero, 2000: Agreement between observed rainfall trends and climate change simulations in the southwest of Europe. *J. Climate*, **13**, 3057–3065, https://doi.org/10.1175/1520-0442(2000)013<3057:ABORTA>2.0.CO;2.

Good, S. A., M. J. Martin, and N. A. Rayner, 2013: EN4: Quality controlled ocean temperature and salinity profiles and monthly objective analyses with uncertainty estimates. *J. Geophys. Res. Oceans*, **118**, 6704–6716, https://doi.org/10.1002/2013JC009067.

Gulev, S. K., M. Latif, N. Keenlyside, W. Park, and K. P. Koltermann, 2013: North Atlantic Ocean control on surface heat flux on multidecadal timescales. *Nature*, **499**, 464–467, https://doi.org/10.1038/nature12268.

Harris, I. P. D. J., P. D. Jones, T. J. Osborn, and D. H. Lister, 2014: Updated high-resolution grids of monthly climatic observations—The CRU TS3.10 dataset. *Int. J. Climatol.*, **34**, 623–642, https://doi.org/10.1002/joc.3711.

Haylock, M. R., P. D. Jones, R. J. Allan, and T. J. Ansell, 2007: Decadal changes in 1870–2004 Northern Hemisphere winter sea level pressure variability and its relationship with surface temperature. *J. Geophys. Res.*, **112**, D11103, https://doi.org/10.1029/2006JD007291.

Hilmer, M., and T. Jung, 2000: Evidence for a recent change in the link between the North Atlantic Oscillation and Arctic sea ice export. *Geophys. Res. Lett.*, **27**, 989–992, https://doi.org/10.1029/1999GL010944.

Hoskins, B. J., I. N. James, and G. H. White, 1983: The shape, propagation and mean-flow interaction of large-scale weather

systems. *J. Atmos. Sci.*, **40**, 1595–1612, https://doi.org/10.1175/1520-0469(1983)040<1595:TSPAMF>2.0.CO;2.

Huang, B., and Coauthors, 2015: Extended reconstructed sea surface temperature version 4 (ERSST.v4). Part I: Upgrades and intercomparisons. *J. Climate*, **28**, 911–930, https://doi.org/10.1175/JCLI-D-14-00006.1.

Hurrell, J. W., 1995: Decadal trends in the North Atlantic Oscillation: Regional temperatures and precipitation. *Science*, **269**, 676–679, https://doi.org/10.1126/science.269.5224.676.

——, and H. van Loon, 1997: Decadal variations in climate associated with the North Atlantic Oscillation. *Climatic Change at High Elevation Sites*, Springer, 69–94, https://doi.org/10.1007/978-94-015-8905-5_4.

——, Y. Kushnir, G. Ottersen, and M. Visbeck, 2003: An overview of the North Atlantic Oscillation. *The North Atlantic Oscillation: Climatic Significance and Environmental Impact*, *Geophys. Monogr.*, Vol. 134, Amer. Geophys. Union, 1–35.

Jeong, J. H., and C. H. Ho, 2005: Changes in occurrence of cold surges over East Asia in association with Arctic Oscillation. *Geophys. Res. Lett.*, **32**, L14704, https://doi.org/10.1029/2005GL023024.

Jin, F.-F., 2010: Eddy-induced instability for low-frequency variability. *J. Atmos. Sci.*, **67**, 1947–1964, https://doi.org/10.1175/2009JAS3185.1.

——, L.-L. Pan, and M. Watanabe, 2006a: Dynamics of synoptic eddy and low-frequency flow interaction. Part I: A linear closure. *J. Atmos. Sci.*, **63**, 1677–1694, https://doi.org/10.1175/JAS3715.1.

——, ——, and ——, 2006b: Dynamics of synoptic eddy and low-frequency flow interaction. Part II: A theory for low-frequency modes. *J. Atmos. Sci.*, **63**, 1695–1708, https://doi.org/10.1175/JAS3716.1.

Jones, P. D., T. Jónsson, and D. Wheeler, 1997: Extension to the North Atlantic Oscillation using early instrumental pressure observations from Gibraltar and south-west Iceland. *Int. J. Climatol.*, **17**, 1433–1450, https://doi.org/10.1002/(SICI)1097-0088(19971115)17:13<1433::AID-JOC203>3.0.CO;2-P.

Jung, T., M. Hilmer, E. Ruprecht, S. Kleppek, S. K. Gulev, and O. Zolina, 2003: Characteristics of the recent eastward shift of interannual NAO variability. *J. Climate*, **16**, 3371–3382, https://doi.org/10.1175/1520-0442(2003)016<3371:COTRES>2.0.CO;2.

Kalnay, E., and Coauthors, 1996: The NCEP/NCAR 40-Year Reanalysis Project. *Bull. Amer. Meteor. Soc.*, **77**, 437–471, https://doi.org/10.1175/1520-0477(1996)077<0437:TNYRP>2.0.CO;2.

Kay, J. E., and Coauthors, 2015: The Community Earth System Model (CESM) large ensemble project: A community resource for studying climate change in the presence of internal climate variability. *Bull. Amer. Meteor. Soc.*, **96**, 1333–1349, https://doi.org/10.1175/BAMS-D-13-00255.1.

Kushnir, Y., W. A. Robinson, I. Bladé, N. M. Hall, S. Peng, and R. Sutton, 2002: Atmospheric GCM response to extratropical SST anomalies: Synthesis and evaluation. *J. Climate*, **15**, 2233–2256, https://doi.org/10.1175/1520-0442(2002)015<2233:AGRTES>2.0.CO;2.

Lau, N. C., 1988: Variability of the observed midlatitude storm tracks in relation to low-frequency changes in the circulation pattern. *J. Atmos. Sci.*, **45**, 2718–2743, https://doi.org/10.1175/1520-0469(1988)045<2718:VOTOMS>2.0.CO;2.

Lee, S. S., J.-Y. Lee, B. Wang, K.-J. Ha, K.-Y. Heo, F.-F. Jin, D. M. Straus, and J. Shukla, 2012: Interdecadal changes in the storm track activity over the North Pacific and North Atlantic. *Climate Dyn.*, **39**, 313–327, https://doi.org/10.1007/s00382-011-1188-9.

Li, J., and J. X. Wang, 2003: A new North Atlantic Oscillation index and its variability. *Adv. Atmos. Sci.*, **20**, 661–676, https://doi.org/10.1007/BF02915394.

Li, S., W. A. Robinson, and S. Peng, 2003: Influence of the North Atlantic SST tripole on northwest African rainfall. *J. Geophys. Res.*, **108**, 4594, https://doi.org/10.1029/2002JD003130.

Limpasuvan, V., and D. L. Hartmann, 2000: Wave-maintained annular modes of climate variability. *J. Climate*, **13**, 4414–4429, https://doi.org/10.1175/1520-0442(2000)013<4414:WMAMOC>2.0.CO;2.

Liu, S., and H. Wang, 2013: Transition of zonal asymmetry of the Arctic Oscillation and the Antarctic Oscillation at the end of 1970s. *Adv. Atmos. Sci.*, **30**, 41–47, https://doi.org/10.1029/2019JC015415.

Lorenz, D. J., and D. L. Hartmann, 2003: Eddy–zonal flow feedback in the Northern Hemisphere winter. *J. Climate*, **16**, 1212–1227, https://doi.org/10.1175/1520-0442(2003)16<1212:EFFITN>2.0.CO;2.

Matsumura, S., S. Ueki, and T. Horinouchi, 2019: Contrasting responses of midlatitude jets to the North Pacific and North Atlantic warming. *Geophys. Res. Lett.*, **46**, 3973–3981, https://doi.org/10.1029/2019GL082550.

Namias, J., 1964: Seasonal persistence and recurrence of European blocking during 1958–1960. *Tellus*, **16**, 394–407, https://doi.org/10.1111/j.2153-3490.1964.tb00176.x.

Ogi, M., Y. Tachibana, and K. Yamazaki, 2003: Impact of the wintertime North Atlantic Oscillation (NAO) on the summertime atmospheric circulation. *Geophys. Res. Lett.*, **30**, 1704, https://doi.org/10.1029/2003GL017280.

——, ——, and ——, 2004: The connectivity of the winter North Atlantic Oscillation (NAO) and the summer Okhotsk high. *J. Meteor. Soc. Japan.*, **82**, 905–913, https://doi.org/10.2151/JMSJ.2004.905.

Oglesby, R., S. Feng, Q. Hu, and C . Rowe, 2012: The role of the Atlantic Multidecadal Oscillation on medieval drought in North America: Synthesizing results from proxy data and climate models. *Global Planet. Change*, **84–85**, 56–65, https://doi.org/10.1016/j.gloplacha.2011.07.005.

Orsolini, Y. J., R. Senan, F. Vitart, G. Balsamo, A. Weisheimer, and F. J. Doblas-Reyes, 2016: Influence of the Eurasian snow on the negative North Atlantic Oscillation in subseasonal forecasts of the cold winter 2009/2010. *Climate Dyn.*, **47**, 1325–1334, https://doi.org/10.1007/s00382-015-2903-8.

Pan, L. L., 2005: Observed positive feedback between the NAO and the North Atlantic SSTA tripole. *Geophys. Res. Lett.*, **32**, L06707, https://doi.org/10.1029/2005GL022427.

Parker, T., T. Woollings, A. Weisheimer, C. H. O'Reilly, L. Baker, and L. Shaffrey, 2019: Seasonal predictability of the winter North Atlantic Oscillation from a jet stream perspective. *Geophys. Res. Lett.*, **46**, 10 159–10 167, https://doi.org/10.1029/2019GL084402.

Peterson, K. A., J. Lu, and R. J. Greatbatch, 2003: Evidence of nonlinear dynamics in the eastward shift of the NAO. *Geophys. Res. Lett.*, **30**, 1030, https://doi.org/10.1029/2002GL015585.

Pinto, J. G., and C. C. Raible, 2012: Past and recent changes in the North Atlantic oscillation. *Wiley Interdiscip. Rev.: Climate Change*, **3**, 79–90, https://doi.org/10.1002/WCC.150.

Qian, B., and M. A. Saunders, 2003: Summer UK temperature and its links to preceding Eurasian snow cover, North Atlantic SSTs, and the NAO. *J. Climate*, **16**, 4108–4120, https://doi.org/10.1175/1520-0442(2003)016<4108:SUTAIL>2.0.CO;2.

Ratcliffe, R., and R. Murray, 1970: New lag associations between North Atlantic sea temperature and European pressure applied to long-range weather forecasting. *Quart. J. Roy. Meteor. Soc.*, **96**, 226–246, https://doi.org/10.1002/qj.49709640806.

Rayner, N. A., D. E. Parker, E. B. Horton, C. K. Folland, L. V. Alexander, D. P. Rowell, E. C. Kent, and A. Kaplan, 2003: Global analyses of sea surface temperature, sea ice, and night marine air temperature since the late nineteenth century. *J. Geophys. Res.*, **108**, 4407, https://doi.org/10.1029/2002JD002670.

Rivière, G., and I. Orlanski, 2007: Characteristics of the Atlantic storm-track eddy activity and its relation with the North Atlantic Oscillation. *J. Atmos. Sci.*, **64**, 241–266, https://doi.org/10.1175/JAS3850.1.

Rodó, X., E. Baert, and F. Comin, 1997: Variations in seasonal rainfall in Southern Europe during the present century: Relationships with the North Atlantic Oscillation and the El Niño–Southern Oscillation. *Climate Dyn.*, **13**, 275–284, https://doi.org/10.1007/s003820050165.

Rodriguez-Puebla, C., A. Encinas, S. Nieto, and J. Garmendia, 1998: Spatial and temporal patterns of annual precipitation variability over the Iberian Peninsula. *Int. J. Climatol.*, **18**, 299–316, https://doi.org/10.1002/(SICI)1097-0088(19980315)18:3<299::AID-JOC247>3.0.CO;2-L.

Scaife, A. A., and Coauthors, 2014: Skillful long-range prediction of European and North American winters. *Geophys. Res. Lett.*, **41**, 2514–2519, https://doi.org/10.1002/2014GL059637.

Seager, R., Y. Kushnir, M. Visbeck, N. Naik, J. Miller, G. Krahmann, and H. Cullen, 2000: Causes of Atlantic Ocean climate variability between 1958 and 1998. *J. Climate*, **13**, 2845–2862, https://doi.org/10.1175/1520-0442(2000)013<2845:COAOCV>2.0.CO;2.

Sun, J., and H. Wang, 2012: Changes of the connection between the summer North Atlantic Oscillation and the East Asian summer rainfall. *J. Geophys. Res.*, **117**, D08110, https://doi.org/10.1029/2012JD017482.

——, ——, and W. Yuan, 2008: Decadal variations of the relationship between the summer North Atlantic Oscillation and middle East Asian air temperature. *J. Geophys. Res.*, **113**, D15107, https://doi.org/10.1029/2007JD009626.

Sung, M.-K., W.-T. Kwon, H.-J. Baek, K.-O. Boo, G.-H. Lim, and J.-S. Kug, 2006: A possible impact of the North Atlantic Oscillation on the East Asian summer monsoon precipitation. *Geophys. Res. Lett.*, **33**, L21713, https://doi.org/10.1029/2006GL027253.

Svensson, C., and Coauthors, 2015: Long-range forecasts of UK winter hydrology. *Environ. Res. Lett.*, **10**, 064006, https://doi.org/10.1088/1748-9326/10/6/064006.

Trenberth, K. E., 1986: An assessment of the impact of transient eddies on the zonal flow during a blocking episode using localized Eliassen–Palm flux diagnostics. *J. Atmos. Sci.*, **43**, 2070–2087, https://doi.org/10.1175/1520-0469(1986)043<2070:AAOTIO>2.0.CO;2.

Trigo, R. M., and J. P. Palutikof, 2001: Precipitation scenarios over Iberia: A comparison between direct GCM output and different downscaling techniques. *J. Climate*, **14**, 4422–4446, https://doi.org/10.1175/1520-0442(2001)014<4422:PSOIAC>2.0.CO;2.

——, D. Pozo-Vázquez, T. J. Osborn, Y. Castro-Díez, S. Gámiz-Fortis, and M. J. Esteban-Parra, 2004: North Atlantic Oscillation influence on precipitation, river flow and water resources in the Iberian Peninsula. *Int. J. Climatol.*, **24**, 925–944, https://doi.org/10.1002/joc.1048.

van Loon, H., and J. C. Rogers, 1978: The seesaw in winter temperatures between Greenland and northern Europe. Part I: General description. *Mon. Wea. Rev.*, **106**, 296–310, https://doi.org/10.1175/1520-0493(1978)106<0296:TSIWTB>2.0.CO;2.

Vicente-Serrano, S. M., and J. I. López-Moreno, 2008: Nonstationary influence of the North Atlantic Oscillation on European precipitation. *J. Geophys. Res.*, **113**, D20120, https://doi.org/10.1029/2008JD010382.

Visbeck, M., E. P. Chassignet, R. G. Curry, T. L. Delworth, R. R. Dickson, and G. Krahmann, 2003: The ocean's response to North Atlantic Oscillation variability. *The North Atlantic Oscillation: Climatic Significance and Environmental Impact*, *Geophys. Monogr.*, Vol. 134, Amer. Geophys. Union, 113–145.

Wallace, J. M., and D. S. Gutzler, 1981: Teleconnections in the geopotential height field during the Northern Hemisphere winter. *Mon. Wea. Rev.*, **109**, 784–812, https://doi.org/10.1175/1520-0493(1981)109<0784:TITGHF>2.0.CO;2.

Walter, K., and H. F. Graf, 2002: On the changing nature of the regional connection between the North Atlantic Oscillation and sea surface temperature. *J. Geophys. Res.*, **107**, 4338, https://doi.org/10.1029/2001JD000850.

Wang, B., R. Wu, and X. Fu, 2000: Pacific–East Asian teleconnection: How does ENSO affect East Asian climate? *J. Climate*, **13**, 1517–1536, https://doi.org/10.1175/1520-0442(2000)013<1517:PEATHD>2.0.CO;2.

Wanner, H., S. Brönnimann, C. Casty, D. Gyalistras, J. Luterbacher, C. Schmutz, D. B. Stephenson, and E. Xoplaki, 2001: North Atlantic Oscillation—Concepts and studies. *Surv. Geophys.*, **22**, 321–381, https://doi.org/10.1023/A:1014217317898.

Wibig, J., 1999: Precipitation in Europe in relation to circulation patterns at the 500 hPa level. *Int. J. Climatol.*, **19**, 253–269, https://doi.org/10.1002/(SICI)1097-0088(19990315)19:3<253::AID-JOC366>3.0.CO;2-0.

Woollings, T., and M. Blackburn, 2012: The North Atlantic jet stream under climate change and its relation to the NAO and EA patterns. *J. Climate*, **25**, 886–902, https://doi.org/10.1175/JCLI-D-11-00087.1.

——, C. Franzke, D. L. R. Hodson, B. Dong, E. A. Barnes, C. C. Raible, and J. G. Pinto, 2015: Contrasting interannual and multidecadal NAO variability. *Climate Dyn.*, **45**, 539–556, https://doi.org/10.1007/s00382-014-2237-y.

——, and Coauthors, 2018: Daily to decadal modulation of jet variability. *J. Climate*, **31**, 1297–1314, https://doi.org/10.1175/JCLI-D-17-0286.1.

Wu, B., and R. Huang, 1999: Effects of the extremes in the North Atlantic Oscillation on East Asia winter monsoon (in Chinese). *Chin. J. Atmos. Sci.*, **23**, 641–651.

——, and J. Wang, 2002: Winter Arctic Oscillation, Siberian high and East Asian winter monsoon. *Geophys. Res. Lett.*, **29**, 1897, https://doi.org/10.1029/2002GL015373.

Xu, T., Z. Shi, H. Wang, and Z. An, 2016: Nonstationary impact of the winter North Atlantic Oscillation and the response of midlatitude Eurasian climate. *Theor. Appl. Climatol.*, **124** (1-2), 1–14, https://doi.org/10.1007/s00704-015-1396-z.

Yang, S., K. Lau, S. Yoo, J. Kinter, K. Miyakoda, and C. Ho, 2004: Upstream subtropical signals preceding the Asian summer monsoon circulation. *J. Climate*, **17**, 4213–4229, https://doi.org/10.1175/JCLI3192.1.

Yin, J. H., 2005: A consistent poleward shift of the storm tracks in simulations of 21st century climate. *Geophys. Res. Lett.*, **32**, L18701, https://doi.org/10.1029/2005GL023684.

Yuan, W., and J. Sun, 2009: Enhancement of the summer North Atlantic Oscillation influence on Northern Hemisphere air

temperature. *Adv. Atmos. Sci.*, **26**, 1209–1214, https://doi.org/10.1007/s00376-009-8148-x.

Zhou, B. T., 2013: Weakening of winter North Atlantic Oscillation signal in spring precipitation over southern China. *Atmos. Oceanic Sci. Lett.*, **6**, 248–252, https://doi.org/10.1080/16742834.2013.11447089.

Zhou, M., H. Wang, S. Yang, and K. Fan, 2013: Influence of springtime North Atlantic Oscillation on crops yields in Northeast China. *Climate Dyn.*, **41**, 3317–3324, https://doi.org/10.1007/s00382-012-1597-4.

Zorita, E., V. Kharin, and H. von Storch, 1992: The atmospheric circulation and sea surface temperature in the North Atlantic area in winter: Their interaction and relevance for Iberian precipitation. *J. Climate*, **5**, 1097–1108, https://doi.org/10.1175/1520-0442(1992)005<1097:TACASS>2.0.CO;2.

Zuo, J., H. L. Ren, B. Wu, and W. J. Li, 2016: Predictability of winter temperature in China from previous autumn Arctic sea ice. *Climate Dyn.*, **47**, 2331–2343, https://doi.org/10.1007/s00382-015-2966-6.